R-phycoerythrin alginate/shellac beads by external gelation: process optimization and the effects of gastrointestinal digestion for nutraceutical applications

Pablo Castro-Varela[1,2*], Mónica Rubilar[3], Antonio Martínez-Férez[4], David Fuentes-Ríos[5], Juan Manuel López-Romero[5], Claudio Alarcon[6], Roberto Abdala-Díaz[1], Félix L. Figueroa[1]

[1]Institute of Blue Biotechnology and Development (IBYDA), Grice-Hutchinson Experimentation Centre, Department of Ecology, Faculty of Sciences, Universidad de Málaga, Spain.

[2]Department of Botany, Faculty of Natural and Oceanographic Sciences, Universidad de Concepción, Chile.

[3]Department of Chemical Engineering, Faculty of Engineering and Sciences, Universidad de La Frontera, Chile.

[4]Department of Chemical Engineering, Faculty of Sciences, Universidad de Granada, Spain.

[5]Department of Organic Chemistry, Faculty of Sciences, Universidad de Málaga, 29017-Málaga, Spain.

[6]Department of Electronic Engineering, Faculty of Engineering and Sciences, Universidad de La Frontera, Chile.

***Corresponding author:** pablo.castro@uma.es

Keywords: alginate/shellac, ionic gelation, simulated gastrointestinal digestion, antiproliferative activity

Abstract

Sarcopeltis skottsbergii is an endemic polar red alga species of South America. Around 20,000 tons of dried algae from this macroalga are produced and sold primarily in Europe and Asia. Modifying the process variables of technologies to protect R-phycoerythrin from macroalgal biomass and the methodology followed are extremely important for maintaining the biotechnology properties of the extracts. This study aimed to evaluate an alginate/shellac mixture as wall material to develop an aqueous phycoerythrin (R-PE) encapsulation system by external gelation and to determine the effect of encapsulation on the properties of R-PE released during simulated gastrointestinal digestion. The Taguchi method was implemented to formulate beads with a high R-PE encapsulation efficiency (EE). The effect of the variables: feeding flow (90 and 20 mL h^{-1}), distance (5 and 10cms), and $CaCl_2$ (5 and 15 g L^{-1}) were optimized, and the bead size, sphericity factor (SF), and total R-PE content were characterized. Finally, the optimal alginate/shellac beads were subjected to *in vitro* dynamic gastrointestinal digestion. The results show that the beads formed under optimal conditions reached an EE value of 97.5%. The $CaCl_2$ concentration and feeding flow most affected the R-PE EE. The release of R-PE from alginate/shellac was affected at acid pH 1; however, the concentration was under 10% of the total R-PE content. A second-order model was tested to describe the release of phycoerythrin from the beads at 1, 3, and 5 pH values. The results showed that the release follows two stages, wall release (stage 1) and core release (stage 2), showing promising targeting properties in terms of time and pH. The R-PE extract and encapsulated R-PE were partially degraded in gastric and intestinal conditions; the mouth did not detect signals from the protein profile. The encapsulation of alginate/shellac led to higher R-PE contents at the end of digestion than non-encapsulated R-PE, suggesting a protective role. Significantly, from permeate streams, equivalent to the absorption of encapsulated R-PE, the bioavailability was 2.5 times higher than non-encapsulated R-PE. NMR results indicate the presence of R-PE and its methyl amino acids and oligosaccharides between 0.5-2.5 and 3.8-6.8 ppm, respectively. A high selectivity index (> 10) was observed for the R-PE extract on the HCT-116 human colon cancer cell line. The alginate/shellac as a wall material and ionic gelation technology used may determine the release of the R-PE pigment at an intestinal site and its antiproliferative effect on health.

1. Introduction

The ability to create a biocompatible wall material that allows for high loading of bioactive agents with no premature release of the payload before reaching the target is crucial to the success of various nano/micro-encapsulation procedures [1,2]. Biocompatibility of the wall matrix, high loading of desired bioactive components, and providing a controlled release mechanism are some factors to consider in the selection of such matrices to serve as an efficacious delivery vehicle [3].

As one of the important classes of food-based encapsulation systems, biopolymeric nano/microparticles can be constructed via a single biopolymer matrix (through the precipitation process of carbohydrates or protein desolvation mechanism) [4]; nanogels of particular biopolymers (e.g., alginate, whey/soy protein, chitosan, etc.) [5,6]; nano-tubes/fibrils of whey proteins [7], or a complexation mechanism of two oppositely charged biopolymers (commonly a protein and a polysaccharide) [8].

Polysaccharide-based capsules are important in encapsulation [9]. Their main functions are the successful encapsulation, transportation, and controlled release of the capsule content to the external environment [10]. For example, alginate is a natural anionic polysaccharide widely used to prepare capsule or pearl encapsulation systems due to its appealing physicochemical properties, biocompatibility, widespread availability, and low cost [11]. The functionality of alginate beads largely depends on their permeability and physicochemical stability. This alginate capsule has a retention and selective release, making it a suitable carrier for biotechnology applications; however, its relatively high porosity is inadequate for some industrial applications [12]. To overcome this problem, blends of alginate and other polymers, such as shellac, may be used to reduce wall porosity [13,14]. Shellac is a natural polymer from the insect *Kerria lacca* and is considered a food additive by the FDA (The United States Food and Drug Administration). In addition, it has a protective effect on gastric fluid, which is an advantage when used in microcapsules to improve probiotic resistance [15]. Thanks to its excellent film forming and protective properties, nontoxicity, and biodegradability, this natural polymer is widely used in adhesives, thermoplastics, sealants, insulating materials, and coating materials in the food and pharmaceutical industries [16] and also used as an oleogelator [17]

In recent years, the shellac biopolymer has attracted significant interest in the development of different encapsulation systems. Experiences have validated its incorporation as an additional external layer to coat capsules [17,18]. The combination of alginate and shellac has been used to protect the aqueous extract of riboflavin by internal

and external gelation [18], microorganisms like probiotics [19] and lipophilic (sunflower oil) compounds to develop an oil encapsulation system by external gelation [20].

Since the extracted algal proteins are intended for human consumption, it is crucial to determine their digestibility under human gastric and intestinal conditions. High digestibility would enable greater absorption of the protein, or its amino acids or short peptides. Given that human digestive proteases have their specificity to bonds near certain amino acids, it is important to verify that human proteases can digest algal protein. Protein digestibility may be assessed by simulating gastrointestinal conditions with standard protocols [21]. Moreover, it is important to highlight that the biological activity of algae proteins may decrease or be modified by the digestive enzymes during their passage through the gastrointestinal tract before crossing the intestinal barrier into the blood circulation system [22]. Additionally, it is crucial to carry out *in vitro* and *in vivo* bioavailability and bioaccessibility studies, as more scientific evidence is needed to support the benefits of algae compounds described to date to validate their efficacy, especially *in vivo* [23].

The phycoerythrin (R-PE) is an oligomeric protein of 240 kDa with three subunits α (about 16 kDa), β (about 21 kDa), and γ (about 39 kDa), and they are bound to specific cysteines by thioether bonds [24]. The study of phycobiliproteins focuses chiefly on therapeutic (bioactive) applications, i.e., the anti-inflammatory, antiviral, hepatoprotective, and anticarcinogenic capacities of R-PE [25–27]. In previous studies in our group, we optimized extraction of R-phycoerythrin pigment from the red alga *Sarcopeltis skottsberggi* by high-pressure homogenization (HPH-assisted extraction). The concentrated extract is characterized by high yield, satisfactory purity, and antioxidant activities.

Considering the potential of the alginate/shellac model system to protect hydrophilic and lipophilic compounds and the advantages of the extrusion and co-extrusion process, this study aimed to develop alginate/shellac beads by external gelation as a model system to encapsulate R-phycoerythrin efficiently, and to evaluate the effect of *in vitro* simulated gastrointestinal digestion and cytotoxic effects on different human tumor lines on R-phycoerythrin beads. The optimal process conditions to prepare beads with efficiency encapsulation (EE) were determined by the Taguchi method with an orthogonal array $L_4(2^3)$. The effect of the variables flow rate, distance, and concentration of calcium chloride ($CaCl_2$) solution on the EE was evaluated. The particle size, release properties, confocal laser microscopy (CLSM), and scanning electron microscopy (SEM) were investigated. The best results obtained under optimal conditions were selected and the parameters of bioaccessibility and bioavailability processes on the simulation gastrointestinal system (SIMUGIT), SDS-PAGE, NMR, and cytotoxic effects on various human tumor lines such as

human colon cancer (HCT-116), human melanoma (G-361), human leukemia (U-937) and in the human gingival fibroblasts cell line (1065SK) were assessed.

2. Materials and methods

2.1 Materials

Alginate and calcium chloride were purchased from Sigma Aldrich (St. Louis, MO). The aqueous shellac solution NORELAC B20 was obtained from Norevo (Germany). NORELAC B20 is a 25% solid ammoniated aqueous shellac solution based on a selected shellac of high and uniform quality refined by solvent extraction. The bioactive, R-phycoerythrin (biliprotein pigment), was obtained from the red alga *Sarcopeltis skottsbergii* after optimization of extraction processes [28].

2.2 Formulation of wall material (WM)

Using a magnetic stirrer, a sodium alginate solution (20 g/L) was prepared by mixing the alginate powder with distilled water under agitation at 700 rpm. The suspension was maintained under gentle agitation (1 h) until complete hydration and left to stand for 60 min for deaeration. The WM was prepared by mixing an alginate solution (20 g/L) and shellac solution (250 g/L), according to Ben Messaoud et al. (2016) with some modifications. Then, the pH of the resulting solution was adjusted to pH 7.5 with 1 M NaOH solution.

2.3 Formulation of beads by external gelation.

Fig. 1 illustrates the process of preparing the alginate/shellac bead system with the bioactive (B). The B/WM ratios (80/20 to 20/80 %v/v) were prepared by mixing the bioactive (R-PE) with the previously prepared WM using continuous agitation (200 rpm for 15 min). The B/WM ratios were extruded by a controlled flow system pump (SyringePump, Inc.) through a 0.3mm nozzle and dripped into 100mL of a gelling bath containing $CaCl_2$ (5-15 g/L) to produce the beads.

The gelling bath was prepared by dissolving the $CaCl_2$ in an ethanol/water mixture (1:1 v/v). The flow rate (30-90 ml/h) and the distance (5-15 cm) from the tips of the syringe to the surface of the gelling bath were evaluated. The beads formed were allowed to stand in the gelling bath for 30 min to ensure crosslinking.

2.4 Experimental design for aqueous encapsulation

An experimental Taguchi design optimized R-PE encapsulation with high EE (%). A matrix L4(2^3) with three independent variables and two levels of work (L1 and L2) was used, applying the criterion 'bigger is better': fed flow solutions of bioactive (R-PE)/WM (flow; L1:20 mL/h; L2:90mL/h), distance to the surface of the gelling bath (distance; L1:5cms; L2:15cms), and concentration of calcium chloride solution ($CaCl_2$; L1:5 and L2:15 g/L). The optimized theoretical equation (OTE) was determined by considering the average of the response with the greatest impact and identifying the most important variables and levels of work.

$$OTE = T + [(V_1, L_1) - T] + [(V_2, L_2) - T] + [(V_3, L_2) - T] \quad (Eq. 1)$$

where V is the variable, T is the average of the experimental run responses, and L is the working levels.

2.5 Determination of encapsulation efficiency (EE) of R-PE load.

The phycoerythrin concentration (R-PE) was determined spectrophotometrically using the Bennett and Bogorad equations [29] as follows:

$$Phycocyanin\ (R-PC) = Abs620 - \left[0.7 * \left(\frac{Abs650}{7.38}\right)\right] \quad (Eq. 2)$$

$$Allophycocyanin\ (A-PC) = Abs650 - \left[0.19 * \left(\frac{Abs620}{5.65}\right)\right] \quad (Eq. 3)$$

$$Phycoerythrin\ (R-PE) = Abs565 - [2.8 * R-PC) - (1.34) * (A-PC/12.7)] \quad (Eq. 4)$$

The encapsulation efficiency of the microcapsule was calculated following the method of Ge et al. [30]with some modifications, by measuring the concentration of non-coated phycoerythrin and the concentration of phycocyanin added at the beginning of the microencapsulation process as follows:

$$EE(\%) = \frac{initial\ concentration\ of\ Phycoerythrin - concentration\ of\ uncoated\ Phycoerythrin}{initial\ concentration\ of\ Phycoerythrin} X\ 100$$

2.6 Sphericity factor (SF) of the beads.

The size and shape of the beads were determined using the ImageJ software (National Institutes of Health, USA). A digital camera coupled to a binocular microscope was used to capture the images of the beads. SF was used to indicate the roundness of the beads, as described by [31], where a value equal to zero indicates a perfect sphere and higher values indicate a greater degree of shape distortion. SF was calculated according to Eq. 5:

$$SF = \frac{Dmax - Dper}{Dmax + Dper} \qquad (Eq. 5)$$

where Dmax is the maximum diameter passing through the bead centroid (mm), and Dper is the perpendicular diameter to Dmax passing through the bead centroid (mm). All samples were assayed in triplicate to determine the mean and standard error. The bead size and shape were determined based on the measurement of 50 beads per sample.

2.8 Mathematical Model of phycoerythrin release

A mathematical model was proposed to describe the results of phycoerythrin release tests. The model proposed was a second-order differential equation which is presented as follows:

$$y''(t) + y'(t)k_1 + y(t)k_2 + x'(t)k_3 + x(t)k_4 + x'(t - t_d)k_5 + x(t - t_d)k_6 = 0 \qquad \textit{(Eq. 6)}$$

In *(Eq. 1)*, x(t) describes the time at which pigment is released from the beads into the aqueous solution since the start at time t=0 up to the end of the experiment. In contrast, y(t) represents the amount of phycoerythrin released measured in percentage units. The starting conditions for x(t), y(t) and their derivative terms were all zero. The Laplace transform was used for obtaining a transfer function *(Eq. 2)* between the input signal x(t) and the output signal y(t) using *(Eq. 1),* with s representing the complex frequency.

$$\frac{Y(s)}{X(s)} = \frac{a_1}{(s+c_1)} + \frac{a_2 e^{-st_d}}{(s+c_2)} \qquad \textit{(Eq. 7)}$$

Where:

$$k_1 = c_1 + c_2 \qquad \textit{(Eq. 8)}$$

$$k_2 = c_1 \cdot c_2 \qquad \textit{(Eq. 9)}$$

$$k_3 = a_1 \qquad \textit{(Eq. 10)}$$

$$k_4 = a_1 \cdot c_2 \qquad \textit{(Eq. 11)}$$

$$k_5 = a_2 \qquad \textit{(Eq. 12)}$$

$$k_6 = a_2 \cdot c_1 \qquad \textit{(Eq. 13)}$$

The second-order transfer function shows a two-step first-order response, with the first occurring at t=0 and the second at t_d. A series of parameters of the release response can

be calculated from the equation, such as the maximum release (M.R) of the first (S1) and second (S2) stage, the time to reach the maximum value or stabilization time (S.T.), and the time delay (t_d) between each phase, calculated as follows:

M.R.S1 = a_1/c_1 *(Eq. 14)*

M.R.S2 = $a_1/c_1+a_2/c_2$ *(Eq. 15)*

S.T.S1 = $5/c_1$ *(Eq. 16)*

S.T.S2 = $5/c_2$ *(Eq. 17)*

Time delay = t_d *(Eq. 18)*

The parameters a_1, a_2, c_1, c_2, and t_d were adjusted to data showing phycoerythrin release at three different pH values: 1, 3, and 5. The parameter adjustment was performed using an evolutive algorithm. The evolutive algorithm considered five parameters, with the minimization of the normalized root mean square error between data and model as the evaluation function, following the algorithm presented by others [32].

2.9 Gastrointestinal-Tract-Simulating Membrane Bioreactor (GITSMB)—SimuGIT

The dynamic gastrointestinal simulator system used (SimuGIT) was developed by the TEP025 Research Group in the Department of Chemical Engineering at the University of Granada [33]. The dynamic *in vitro* Gastrointestinal-Tract-Simulating Membrane Bioreactor GITSMB (SimuGIT), consists of a continuous stirred-tank reactor (CSTR) connected in series to a continuous plug-flow tubular reactor (PFTR) equipped with a monochannel tubular ceramic microfiltration membrane. The CSTR used to simulate gastric digestion in the stomach is a benchtop fermenter supplied by Braun Biotech International (Biostat B). It comprises a conventional autoclavable stirred tank glass vessel equipped with an impeller stirrer (Rushton 180 W) and a proportional-integral-derivative (PID) unit control system for the temperature, level, foam, dissolved oxygen, and pH. The control system unit includes an RS-422 interface that enables the control of the CSTR with a computer. The CSTR has an external jacket to maintain a constant temperature, such that the temperature in the vessel is measured using a Pt-100 digital sensor and is accurately controlled (Tsetpoint ± 0.1 ◦C) by the PID loop connected to a thermostatic laboratory bath. The CSTR system also has sampling and reagent addition inlets using several peristaltic pumps (Eyela, MP-3). The pH inside the CSTR is measured by a pH electrode (Hamilton, Easyferm Plus K8) immersed in the vessel and adjusted by a pH control system made by the authors based on data acquisition modules, which acts on two different peristaltic pumps that dose the acid and basic solutions (HCl or $NaHCO_3$). The digested solution exiting the CSTR is continuously driven to the PFR. To this end, the PID control system acts on impulsion and return peristaltic pumps (two of the four peristaltic

pumps integrated into the benchtop fermented, as previously described), such that by varying the flow rates of these pumps, the pressure inside the hydraulic circuits and the product filtration rate can be regulated. In addition to this self-developed control pressure mechanism, the operating pressure can be adjusted accurately (P setpoint ± 10 mmHg) with a spring-loaded pressure-regulating valve (SS-R4512MM-SP, Swagelok) and monitored by a digital pressure gauge (Endress + Hauser, Ceraphant PTC31). The continuous PFR connected in series to the CSTR serves for the simulation of the conditions in the intestine. It consists of a stainless-steel cylindrical tube (provided by Prozesstechnik GmbH, Basel, Switzerland) equipped with a monochannel ceramic microfiltration (MF) membrane in a tubular configuration provided by Atech Innovations GmbH. The MF membrane used for the experiments is an inorganic one of α-Al_2O_3 active surface with a mean pore diameter equal to 0.2 µm and molecular weight cut-off of 1.2 kDa (model 20N). The dimensions of the selected membrane are 1000 mm in length, 6 mm in duct diameter, and 2 ± 0.5 mm in thickness. This type of MF membrane also ensures a series of advantageous characteristics, such as high resistance to temperature (suitable for steam sterilization at 121◦C) and pressure (up to 10 bar) during the cleaning protocols, pH stability (0 to 14), possibility of back pulsing, very high abrasion resistance (against aggressive chemical reagents), optimal permeability recovery, high selectivity and performance, and long lifetime service. The PFR is integrated with the CSTR using a drive and return system made of chemically resistant polyethylene tubes. Finally, a precision electronic mass balance with USB connectivity (Sartorius, Quintix 5102, accuracy equal to 1 mg) is coupled to an automatic sampling and data registration system to register permeate values (the bioaccessible fraction that crossed the membrane) over time.

2.9.1 GITSMB Conditions

- Gastric Phase

When the trial began, the bath temperature that kept the reactor jacket warm was set at 37.5 ± 1°C throughout the process, and the reactor stirring speed was set at 50 rpm to simulate the peristaltic movements of the stomach. Next, 800 mL of GSF and 14 mL of SSF were prepared using the reagents mentioned in Section 6.5. The concentrations of each reagent for each fluid were pre-established according to Brodkorb et al. [34]. Once prepared, the GSF was introduced into the reactor and heated to 37.5°C. The pH dropped to 3 at this point, as the empty stomach was simulated before adding the food with the microcapsules. At the same time, 20 g of mineral water were weighed, and 1g of phycoerythrin was added. Two separate tests were carried out as two different samples (encapsulated and nonencapsulated phycoerythrin) were chosen. The SSF was then mixed with the food preparation + microcapsules; 1 mL alpha-amylase solution (75 U/mL), 0.1

mL $CaCl_2*2H_2O$ of concentration 0.3 M, and 4.9 mL distilled water were added (final salivary fluid to food preparation ratio of 1:1). The mixture was shaken for 2 min, and the pH was adjusted to 7 (if necessary). Once the GSF was hot, the mixture of the food with the SSF was added to the reactor tank, stirred for a few seconds, and an initial sample was taken. Then, a 10 mL solution of pepsin (2000 U) and 50 mg of phospholipid (Lipoid p45) were added, and the pH was adjusted to 3 by controlled dosing of 6 M HCl. From then on, a sample was taken every 5 min for the next 30 min.

- Duodenum Phase

When the gastric phase ended with the last sample taken, the pH of the GSF was raised to 6.5 by dosing 1 M NaHCO3 at a rate of 2.05 mL/min, and a sample was taken after adjustment. This pH simulates the action of pancreatic juices on the food being digested. Intestinal enzymes were added: 10 mL solution of pancreatic lipase (2000 U/mL), biliary salts (for a final concentration of 5 mM), 10 mL solution of pancreatin (10%), and 1 mL solution of trypsin (50 mg/assay). Digestion in the duodenum takes about 10 min after adding enzymes, and a sample was taken after that digestion period. The approximate total duration of this phase (including pH rise, addition of enzymes, and digestion) was 30 min.

- Intestinal Absorption Phase

To simulate intestinal absorption, fluids from the bioreactor were pumped to flow through the modular filtration system. A 0.2 µm membrane size was chosen for these trials based on previous tests [35,36]. The system overpressure limit was set at 50 mmHg, so that the diffusion of phycoerythrin through the membrane was due solely to passive transport. It is important to remember that the ionization characteristics of a compound can profoundly affect the rate of its transfer by passive diffusion because only the unionized species are capable of passive diffusion across the membrane. Once the circuit was primed and fluids began to fall into the bioreactor, the intestinal absorption phase was considered to have begun and lasted 180min. Samples were taken at 30, 60, 90, 120, 150, and 180 min. Two samples were taken each time, one from the fluid filtrated through the membrane (permeate) and another from the retained fluid, which forms part of the colonic residue (retained).

In summary, each simulation test lasted approximately 4 h: Gastric phase (30 min), duodenal phase (30 min), and intestinal absorption phase (180 min). Each trial was conducted in duplicate. Throughout the trial, the system program generated a data file recording all the events and processes during the simulation. This file was then processed in the computer to obtain information on all the variables.

2.9.2 Analysis of the Samples

All samples collected during the assay were refrigerated. Subsequently, the concentration of phycoerythrin present in the fluids in each sample was measured using spectrophotometry analysis according to Bennett & Bogorad, [29], polyacrylamide gel electrophoresis (SDS-Page) and nuclear magnetic resonance (NMR). The concepts of release or bioaccessibility and bioavailability were used to measure the amount of phycoerythrin released along the digestive tube in the chymus and the amount absorbed by the membrane, respectively. The release corresponds to the pigment fraction delivered by microcapsules to the gastrointestinal tract during the gastric and duodenal phases and was calculated using Equation (6), adapted from Rivas-Montoya et al. [33]. When release and precipitation processes took place simultaneously, the same equation was used to calculate the bioaccessible percentage as the released and non-precipitated fraction in the chymus. On the other hand, bioavailability corresponds to the pigment fraction absorbed by diffusion through the membrane during the intestinal absorption phase and was calculated using Equation (7), adapted from Ariza et al. [37].

$$Bioaccesibility\ (\%)\frac{pigment\ phycoerythrin\ in\ chymuss}{initial\ pigment\ phycoerythrin\ in\ microcapsules}x100 \qquad (Eq.19)$$

$$Bioavailability\ (\%)\frac{phycoerythrin\ amount\ in\ IAS}{initial\ pigment\ phycoerythrin\ in\ microcapsules}x100 \qquad (Eq.20)$$

where IAS means intestinal absorption samples. In both equations, the amounts of phycoerythrin in the chymus and the microcapsules are expressed in milligrams of R-PE by total biomass (mg g^{-1}).

2.9.3 SDS polyacrylamide gel electrophoresis (SDS–PAGE):

The hydrolysates of the encapsulated and non-encapsulated phycoerythrin were prepared for SDS-PAGE using the protocol developed by [38], which combines TCA/acetone and methanol washes and a phenol step for protein extraction. SDS-PAGE will be performed according to Laemmli's procedure [39].

2.9.4 Nuclear magnetic resonance (NMR)

A 400 MHz Plus Avance II NMR spectrometer (Bruker, Switzerland) was used for nuclear magnetic resonance analyses. ^{1}H NMR spectra were recorded at 400 MHz at room temperature (21 ºC). Samples (15-30 mg) were dissolved in deuterated dimethyl sulfoxide (DMSO-d_6, 0.75 mL), with residual solvent peaks at δ= 2.50 (DMSO) and δ= 3.42 (H_2O) ppm for ^{1}H. In some samples, D_2O (3 drops) was added.

3.0 Cell Cultures

To perform the cytotoxicity analysis, the five following cell lines were chosen: human fibroblasts (1064sk, CIC-UGA, ES), human leukemia cell line (U-937, ATCC, USA), human malignant melanoma (G-361, ATCC, USA), and colon cancer cell line (HCT-116, ATCC, USA) stored in liquid nitrogen in the cell culture unit of the Central services for research support (SCAI) of Malaga University (UMA). To maintain the cells, 1064sk, G-361, and HCT-116s were previously cultured using Dulbecco's modified Eagle's medium (DMEM) (Capricorn Scientific, ref. DMEM-HPSTA) supplemented with 10% fetal bovine serum (Biowest, ref. S1810-500), 1% penicillin-streptomycin solution 100× (Capricorn Scientific, ref. PS-B), and 0.5% of amphotericin B (Biowest ref. L0009-100). U-937 were grown in RPMI-1640 medium (BioWhittaker, ref. BE12-167F) supplemented with 10% fetal bovine serum (Biowest ref. S1810-500), 1% penicillin-streptomycin solution 100×, and 0.5% of amphotericin B. The cells in suspension (U-937) were harvested upon reaching 70–75% confluence and centrifuged at 1500 rpm for 5 min at room temperature. Once centrifuged, the corresponding test or the subculture of the cells was carried out. The cells were kept under subconfluence in an atmosphere-controlled incubator with 5% CO_2 at 37 °C.

3.1 Analytic Method (MTT assay)

For the cancer and healthy cell viability assay, U-937, HTC-116, G-361, and 1064sk cells were incubated at encapsulated R-PE concentrations of 5 to 4.76 × 10^{-6} mg mL^{-1} in serial dilutions (1:1) from the alga *S. skottsbergii*. The experiment was conducted individually with each cell line in a 96-well microplate for 72 h (37 °C, 5% CO_2 in a humid atmosphere). The proliferation of these cell lines was estimated by the MTT (3-(4,5-dimethylthiazol- 2-yl)-2,5-diphenyltetrazolium bromide) assay [40]. Briefly, 10 µL of the MTT solution (5 mg mL^{-1} in phosphate-buffered saline) was added to each well. The plates were incubated at 37 °C for 4 h. The yellow tetrazolium salt of MTT was reduced by mitochondrial dehydrogenases of metabolically active viable cells to form insoluble purple formazan crystals. Formazan was dissolved by adding acid-isopropanol (150 µL of 0.04 N HCl–2 propanol) and measured spectrophotometrically at 550 nm (Micro Plate Reader 2001, Whittaker Bioproducts, USA). The relative cell viability was expressed as the mean percentage of viable cells compared to the untreated cells. Four samples for each tested concentration were included in each experiment. Measurements were taken in independent experiments in triplicate.

3.3 Calculation of the selectivity index (SI)

The selectivity index determines the cytotoxic selectivity of the compounds tested and is calculated by the ratio between the IC_{50} as indicated in the following formula:

SI = (IC 50 OF health cell)/(IC 50 of cancer cell)

[41] state that a selective compound presents a SI over 3.

4.0 Results

4.1 Optimization of the encapsulation process

The different combinations of alginate and shellac were tested for the liquid-core matrix. Only the formulation alginate/shellac (75/25 %V/V) was satisfactory in determining the basic process conditions of bead preparation. Thus, the effect of the process variables (flow rate, distance, and concentration of $CaCl_2$) on the EE of R-PE was investigated (Figure 1). For this, 80 % of alginate/shellac mixture (wall material) was mixed with 20 % of R-PE extract, and then extruded and dripped into $CaCl_2$ solution for 30min of gelation to form beads. The R-PE encapsulation process was optimized where included the effect of three independent variables, flow rate (90 and 20 ml min^{-1}), distance (10 and 5 cm), and $CaCl_2$ (5 and 15 g L^{-1}) on %EE were evaluated. Table 1 shows the results of EE (%), particle size, and SF obtained under different conditions. The EE values ranged between 89 and 97%. From the Taguchi design, a higher $CaCl_2$ concentration, lower flow rate, and high distance resulted in a high EE.

Figure 1 shows the effect of the working levels of each variable on the encapsulation efficiency (degree of incline of the slope as a response to EE). The greater the difference between levels 1 and 2 for a variable, the higher the change magnitude of the response. The variable $CaCl_2$ showed a greater influence on the EE with an average difference of 7.0 units between the responses of working-level 1 (L1:5 g L^{-1}) and working-level 2 (L2:15 g L^{-1}), followed by the variable distance, showed an influence on the EE with a difference of 1.50 units between the levels. The variable flow rate with a difference of 0.5 units between the two working levels. Therefore, the variable $CaCl_2$ presented the highest difference between flow rate and distance. Thus, the R-PE pigment can be more efficiently encapsulated in beads coated with a low $CaCl_2$ (<15 g L^{-1}) due to the formation of an encapsulating matrix where coating the capsules by Ca^{2+} reticulation of shellac leads to the formation of a uniform and smooth layer at the surface of alginate capsules compared to capsules prepared at 15 g L^{-1} of $CaCl_2$, generating the formation of a non-uniform external layer.

The coefficients of determination (R^2) for the independent variables flow, distance, and $CaCl_2$ were 2.5, 4.2, and 90.7%, respectively. The coefficient of determination for these three variables was significant ($p < 0.05$) with R^2 = 97.4% indicating a good affinity or association of the independent variables with the EE. The optimized theoretical equation (OTE) for EE was determined using Eq (1), where T is equal to 97 %, which is the total

average of the response of experimental runs, and L is the working levels of the equation. The OTE contributed to 97 % of the response, coinciding closely with the optimal experimental value (Point N°1: 97.5 %). These results confirmed that combining the control variables and working levels was sufficient to determine an optimum.

4.2 Sphericity factor (SF) and scanning electronic microscopy of the beads

The fluorescence observation and scanning electronic microscopy of the aqueous-core alginate/shellac capsules are shown in Figures 2 and 3, respectively. Figure 3 shows SEM images of optimal alginate/shellac beads from design point 1, which reached the highest EE. The image shows that the bead surfaces are smooth and free of pores, which is important for the stability of the beads because the pores facilitate the exit or loss of the R-PE. However, the beads from design point 2 and 3 shows non-uniform particles and rough surfaces. Figure 2 shows the R-PE distribution in the beads observed by CLSM. The R-PE pigment was identified by the fluorescence of the chromophores group after the external gelation process. A high-intensity fluorescence was emitted, homogeneously distributed throughout the polymeric matrix in all design points. According to the design points, the bead size was 10-50 mm. Additionally, the lowest SF value was found in design point 1, reaching 0.04, whereas design point 3 showed the highest SF value at 0.358. According to Chang et al. (2011), beads with an SF value lower than 0.05 are considered spherical beads. Thus, semi-spherical beads were obtained in our study. Additionally, the irregular head shape was observed with high distance (10 cm) and high $CaCl_2$ (15 g L^{-1}), which correspond to the EE decrease (Table 1).

4.3 Bioavailability and bioaccessibility of R-PE

Figure 4 shows the bioaccessibility of encapsulated and non-encapsulated R-PE during intestinal digestion. The encapsulation of R-PE significantly influenced the bioaccessibility and bioavailability of pigment R-PE. The bioaccessibility of R-PE extract was significantly higher than alginate/shellac microparticles, reaching values around 30.4 % at 180 min, whereas the bioaccessibility from encapsulated R-PE was detected in the gastric and intestinal phases, and reached values of 20.25 % at the end of the intestinal digestion (180min).

The bioavailability of encapsulated and non-encapsulated R-PE at the end of intestinal digestion is presented in Figure 5. Comparing R-PE samples, we observed that encapsulated R-PE presented the highest percentages (6.0%) of bioavailability when compared to non-encapsulated R-PE (2.41%) at 180min of intestinal digestion. At the beginning of the intestinal absorption phase (permeate samples), it was noted that small percentages of non-encapsulated and encapsulated R-PE from the initial total content were

available and passed through the membrane. We observed during each digestion time for all samples was increased the R-PE content showed similar contents, but at the end of the intestinal digestion, a significant difference was detected at 180min reached for non-encapsulated and encapsulated R-PE 0.123 and 0.31 mg of R-PE g^{-1} of biomass, respectively.

4.4 SDS-PAGE, phycoerythrin release, and NMR Spectra.

Figure 6 outlines the SDS-PAGE profile of the different stages of the digestion samples, where multiple protein bands ranging from 20 to 100 kDa can be observed, except for the mouth and stomach. More intense bands eluted in the duodenum and intestine at around 50, 20-37kDa, suggesting that some bands correspond to Phycoerythrin. Thus, it is possible to understand that the matrix core of the encapsulation of the phycoerythrin has good resistance to mouth and stomach levels because no signal was reported. However, signals between the concentrated and permeated phases in the intestine are similar in the intense bands at different reaction times (30 and 180min). Finally, it is feasible to suggest that phycoerythrin has a good controlled release in the function of matrix encapsulation formulated at the intestinal level. These results have a good coincidence with the release test evaluated in different pH (1-5), where the encapsulated R-PE at pH 1 does not exceed 10% of release content, while at pH 3 and 5 it remains, which may suggest a controlled release after 180 min of exposure from the encapsulating matrix (Figure 7A).

Figure 7B presents the phycoerythrin release as a percentage of the total value with respect to time, modeled using a second-order differential equation representing a two-step first-order release response. The image shows that the release takes place at two different stages, each describing a first-order response, resulting in an overall second-order response. The first stage occurs from t=0, corresponding to pigment release from the wall. The pigment concentration from the wall release then reaches a maximum value at a specific moment, after which no further release occurs until the next stage begins. Stage 2 shows a release restart, which releases the remaining pigment from the bead core. From Table 3 a series of parameters related to the response were calculated from the Laplace representation and shown in Table 4. The results suggest that the release can be described by two stages: wall release (stage 1), with maximum values 273.2±35.5% higher in stages 1 than those of pH 3 and 5, and core release, with maximum values 294.0±36.8% higher than the values obtained for pH 3 and 5. Core release (stage 2) for pH =1 started 26.3±2.6 min after stage 2 started for pH 3, 5.

To carry out the ^{1}H NMR analyses, samples E1/FI and E1/IP were dissolved in DMSO-d_6. The ^{1}H NMR spectra recorded for both samples are very similar (Figures 8, A, and B). In

both spectra, between 3.8 and 6.8 ppm, the singlets can clearly be seen due to the hydroxyl group protons (OH) present in the oligosaccharide structure. In the interval 2.5 and 0.5 ppm, the signals associated with the aliphatic protons of methyl groups of amino acids (alanine (Ala), leucine (Leu), isoleucine (Ile), and valine (Val)) are present in proteins (Figure 8). Moreover, signals observed at 5.7, 6.7, 7.0, and 7.2 ppm can be assigned to phycoerythrin double bonds (pyrrole skeleton). The presence of oligosaccharide hydroxyl groups was confirmed by recording the ^{1}H NMR spectra in a mixture of deuterated DMSO and D_2O as solvents. In this case, OH signals are not observed (Figure 8).

4.5 Cell Viability of Lines HTC-116, G-361, U-937 and 1064SK

The cytotoxicity of encapsulated and non-encapsulated R-PE (aqueous extract) was determined in the human cancer cells (HCT-116; G-361; U-937) and healthy cells (1064sk). After treating the cells with increasing concentrations of the two samples, cell proliferation was evaluated using an MTT assay. As shown in Table 2, all the samples exhibited relative inhibition ratios at all concentration levels and demonstrated a dose-dependent inhibition in the growth of cancer cells. The lowest IC_{50} value in G-361 with encapsulated R-PE was 4132 ± 10.86 µg mL^{-1}, in U-937 IC50 cells was 1251 ± 4.83 µg mL^{-1}, in HCT-116 IC_{50} cells was 1076 ± 8.46 µg mL^{-1} (Table 2). For R-PE aqueous extract (non-encapsulated), the lowest IC_{50} value in HCT-116 cells IC_{50} was 144.5 ± 3.96 µg mL^{-1}, while in U-937 IC50 was 2788 ± 11.5 µg mL^{-1} and in G-361 was 2702 ± 12.6 µg mL^{-1} (Table 2). On the other hand, in the healthy cells line in 1064sK, the encapsulated and non-encapsulated R-PE were 3516 ± 15.3 µg mL^{-1} and 4438 ± 10.3 mg mL^{-1}, respectively. The highest SI values calculated for encapsulated R-PE also belonged to the three above-mentioned cell lines, including HCT-116 (> 3.27), U-937 (> 0.86), and G-361 (> 0.26), compared to the other cell lines (Table 2). The SI values calculated for the R-PE extract for all the cell lines were high, ranging between 30.71 and 1.59, depending on the cell line, indicating higher effectiveness of the R-PE extract on the cancer cell lines compared to the encapsulated R-PE. These results have a cytotoxic effect on cancer and healthy cells, where the R-PE aqueous extract presented relatively high antitumor activities against HCT-116 cells.

5.0 Discussion

Algae, especially macroalgae, have recently emerged as a vast source of metabolites with unique structures and nutritional and therapeutic activities, and this field is becoming one of the hot challenges in food science and technology [23]. Our work is the first approach in a new generation of potential ingredients based on alginate/shellac as biomaterials for

protecting R-PE to maintain biological activity and bioavailability under human physiological conditions. To formulate the wall material, alginate/shellac has been validated by other authors with good results in the efficiency of encapsulation for bioactive like riboflavin [18], sunflower oil [20] and inclusive in a microorganism [19]. However, the protection processes for phycobilin pigments have been little explored but have great potential in the food industry, according to several studies [42–44]. In this sense, the R-PE was successfully encapsulated by Taguchi optimization, which revealed that the high efficiency is given with design point 1, reaching values close to 97.5 ± 0.71 % EE (Table 1). Similar results were obtained by Pan-tai et al. [45] for phycocyanin (C-PC), from the microalga *Arthrospira platensis* (Cyanobacteria), under alginate formulation process to beads by ionic gelation reached 98% EE. It was found that alginate and $CaCl_2$ concentration have a significant influence on the EE (%) and bead properties. In the same line, Yan et al. [46] developed a wall material by an extrusion method using alginate and chitosan as coating materials for the protection of the phycocyanin from *Arthrospira platensis* (Cyanobacteria), which reached values around 56 % of EE. These values are lower than our results, where the differences may be due to the combination of the materials and the low concentration of $CaCl_2$ (2.5 %), in which the competition between the two polymers to bind Ca^{2+} calcium ions affects the final composite gel structure. The observations of Messaoud et al. [18] found that coating the capsules by Ca^{2+} reticulation of shellac led to the formulation of a uniform and smooth layer that was closely related to the amount of shellac and Ca^{2+}, were recommended concentration of $CaCl_2$ 2 % (%W/V). Also, Henning et al. [47] suggest that concentrations of $CaCl_2$ over 2 % (%W/V) are enough to ensure the formation of cross-linked hydrogel alginate/shellac membranes. However, there found a shrinking phenomenon of the alginate hydrogels during the coating process. This shrinking might be induced by the depletion of cross-linked calcium ions in the alginate hydrogel due to chemical reactions between the calcium ions and the shellac. From our observations, we suggest that the range of $CaCl_2$ between 5 and 15 % (%W/V) depends directly on the interaction with shellac, found high EE values (97.5%) at 5 % (%W/V). Further studies are needed for another aspect that could describe the differences in the thickness of the shellac layers being linked to the total amount of H^+ ions in the capsules (adjusted by the pH value).

The SEM and fluorescence observation of alginate/shellac beads exhibited a semi-spherical shape thanks to the intrinsic properties surface tension, density, and viscosity of the $CaCl_2$ solution before the encapsulation stage [20,48]. According to Chan [31], beads with SF values lower than 0.05 are considered spherical beads. Therefore, the beads in our study are semi-spherical. The irregular bead shape was observed with a high distance (10 cm) and high $CaCl_2$. However, the bead morphology became spherical as the distance of

extrusion and $CaCl_2$ on the %EE increased. According to Chan et al. [48], SF was an efficient tool as a sphericity indicator to study the shape of the beads. Additionally, spherical beads as an encapsulation system are more stable than irregular or non-spherical shaped beads, as spherical beads have a low surface/volume ratio, producing a lower diffusion of bioactive in the beads. Dried microcapsules presented diameters ranging from 0.8 to 1.20mm (Table 1). Despite the large size, these microcapsules may be used in solid foods such as chocolate and cereal bars where the texture is not affected by the particle size [19].

The alginate/shellac beads with the highest EE were subjected to the *in vitro* dynamic digestion method (SIMUGIT). The percentage of R-PE found in the permeate stream was lower than in the encapsulated R-PE, where we found 6.0 % of bioavailability at 180 min of intestinal digestion. The R-PE bioavailability differed significantly depending on the wall material; after the gastric step, the alginate/shellac beads contained 0.58mg g^{-1} of R-PE, a decrease of 89.6 % compared to the initial concentration (5.58 mg g^{-1}). In the same vein, in the intestinal stage, the content available and passed through the microfiltration membrane (0.05 μm) more R-PE was seen to be released, showing a decrease of 94.5 % of R-PE compared to the initial concentration. Thus, the alginate/shellac as wall materials for R-PE has an acceptable mechanism for protecting the pigment, which allows it to pass through the mouth, stomach, and duodenum barriers and releasing the compound in a controlled intestinal phase. According to Pimentel et al[23], enriching protein extracts from *Porphyra dioica* (Nori) released at the intestinal level is advisable because it is in the intestine where the proteins are degraded by enzymes and peptides are absorbed into the bloodstream, thereby improving the antioxidant activity. Our DGGE analysis showed that the fraction of the final digest was between 25-50KDa, where the profile of the extracted protein is consistent with previous results reported by Pimentel et al[23] and Stack et al. [49] for red algae. Similar conclusions were reported by Wu et al. [50], who evaluated the *in vitro* digestion of R-PE and found that the final intestinal digestion still contained high antioxidant activity in proteins fraction of <3 kDa. They indicate that digestion-resistant antioxidant peptides of R-PE may be obtained by *in vitro* gastrointestinal proteinase degradation. Likewise, Yabuta et al. [51] found that the R-PE from *Porphyra* sp extract is readily digested to release the phycoerythrobilin compound during the gastrointestinal digestion process of mammals. They also suggested that the various therapeutic activities of phycoerythrin appear to be associated with the phycoerythrobilin compound released during mammalian gastrointestinal digestion. On the other hand, Teixé-Roig et al. [52] reported that the other phycobiliprotein C-phycocyanin (C-PC) was protected by double emulsions containing pectin and sodium alginate presented high %EE and the most suitable to prevent phycocyanin degradation during the digestion process. This suggests

that biological activity and safety can be enhanced after digestion. Also, Campos et al. [53] reported that the same C-phycocyanin (C-PC) extract could be applied as a stable blue dye in ice creams and highlight the increased antioxidant activity of the C-PC-added products after *in vitro* simulated digestion.

A second-order model was proposed for describing the Phycoerythrin release into an aqueous solution. The proposed model used differs from first-order models presented by other researchers [18]. The second-order model described two stages, each described by a first-order response and separated by a time delay. The first stage corresponded to wall release diffusion, and the second to pigment release from the core. Regarding the maximum release values, pH=1 showed a higher maximum 273.2 ± 35.5 % and 294.0 ± 36.8 % in comparison to those of pH 3 and 5 for stages 1 and 2, respectively, with core release (stage 2) starting 26.3±2.6 min after stage 2 have started for pH 3, 5, showing promising targeting properties with respect to time and pH. The results suggest that time and pH modify the release of the pigment from the alginate matrix, showing potential for targeting areas characterized by certain pH and retention time. Regarding using a unit step signal as input to the second-order differential equation for describing the release of pigment, this input signal selection could have been changed to a more straightforward Dirac impulse function. This is because the integration of the Dirac impulse function can be made equivalent to the unitary function. However, this would have required using a third-order differential equation to describe the release, making the proposed model more complex.

Unfortunately, the changes in R-PE concentration through digestion have low reports in the literature. But it is clear that the biological activities of R-PE are maintained after the *in vitro* digestion stage demonstrated by Yabuta et al. [51], Wu et al. [50], Stack et al. [49], and Pimentel et al. [23]. Our research shows that the amount of encapsulated R-PE released in the final stage of intestinal digestion (0.31 mg g^{-1}) is sufficient to cause a cytotoxic reaction against human cancer cells. The IC_{50} values for HCT-116 (1076 ± 8.46) and U-937 (1251 ± 4.83), as well as the SI values for the R-PE, encapsulated in these cells (> 3.27 for HCT-116 and > 0.86 for U-937) suggest encapsulated as a promising therapeutic candidate, particularly on gastro and blood cancers. Knowing that the greater the SI value is, the more selective it is, and SI values over 3 indicate general toxicity [41], we concluded that compared to encapsulated R-PE, (SI: 30.71), R-PE extracts non-encapsulated are better candidates for growth suppression of all the examined cell lines with SI values > 3. These observations can be attributed to the wall materials (alginate/shellac) possibly affecting the growth factors of human cells, primarily due to alginate, which has been shown to have catalytic characteristics in human cells [54]. Future

studies in an *in vivo* system are needed to relate antiproliferative and antioxidant activities as potential nutraceuticals.

6.0 Conclusions

This study provided insights into the process conditions to prepare beads with a high EE of R-PE and the evolution under *in vitro* gastrointestinal digestion microcapsules. The variables process for R-PE encapsulation was obtained using a feeding flow of 20mL h^{-1}, 5 cm of distance, and 5 gr L^{-1} of $CaCl_2$. The encapsulation under optimal conditions showed 97.5% showing a good coincidence with the predictive OTE values (97 %). The beads presented a semi-spherical shape and were free of pores with a size of 1.2 mm. The *in vitro* digestion showed that the alginate/shellac beads were 2.5 times higher in bioavailability than non-encapsulated R-PE extract at intestine stage digestion with a concentration of 0.31 mg of R-PE. Finally, the R-PE charged in the encapsulate can be used as a potential delivery system for aqueous extract and give a therapeutic response according to the IC_{50} (144 μg mL^{-1}) values found for the R-PE for colon cancer. We suggest that the encapsulation system of R-PE can be incorporated into a food matrix for nutraceutical applications.

Credit authorship contribution statement

Conceptualization, P.C-V., M.R., F.L.F. and R.A-D.; methodology C.A. and P.C-V.; mathematical model methodology, C.A; SIMUGIT methodology, A.M-F.; SIMUGIT supervision and writing A.M-F.; NMR methodology, D.F-R and J.M.L.; NMR experiment supervision and writing, J.M.L; data curation, C.A and P.C-V; validation, P.C-V; writing original draft preparation, P.C-V.; writing-review and editing, P.C-V., M.R., F.L.F. J.M.L., A.M-F., and R.A-D.; visualization, P.C-V; supervision, M.R., F.L.F. and R.A-D. All authors have read and agreed to the published version of the manuscript.

Declaration of competing interest

The authors declare that there are no conflicts of interest.

Data availability

The data that support the findings of this study are openly available from the corresponding author [P.C-V.] on request if the editor or reviewer needs it.

Acknowledgments

We gratefully acknowledge the Department of Chemical Engineering of the University of Granada and the IBYDA Center of the University of Malaga for resource and technical support. P.C.V. thanks the Asociación Iberoamericana de Postgrado (AUIP) and the University of Malaga for PhD scholarship research. We also want to thank Mr. Jaime Zamorano from GELYMAR Company (Chile) and NOREVO Company (Germany) for collaborating on this research project.

Funding information

This study was supported by the Project "Blue nutricosmeceuticals with cyanobacteria and macroalgae (NAZCA)-Nutricosmeceútica azul con cianobacterias y algas (NAZCA-) PY20-00458 by the Andalusian Government, Spain.

References

[1] E. Assadpour, S.M. Jafari, Importance of release and bioavailability studies for nanoencapsulated food ingredients, Release and Bioavailability of Nanoencapsulated Food Ingredients. (2020) 1–24. https://doi.org/10.1016/B978-0-12-815665-0.00001-1.

[2] H. Rostamabadi, E. Assadpour, H.S. Tabarestani, S.R. Falsafi, S.M. Jafari, Electrospinning approach for nanoencapsulation of bioactive compounds; recent advances and innovations, Trends Food Sci Technol. 100 (2020) 190–209. https://doi.org/10.1016/J.TIFS.2020.04.012.

[3] S.R. Falsafi, S.P. Bangar, V. Chaudhary, E. Hosseini, Z. Mokhtari, A.C. Karaca, M.K. Samota, D. Goswami, V. Krishnan, G. Askari, H. Rostamabadi, Recent advances in oral delivery of bioactive molecules: Focus on prebiotic carbohydrates as vehicle matrices, Carbohydr Polym. 298 (2022) 120074. https://doi.org/10.1016/J.CARBPOL.2022.120074.

[4] I.J. Joye, D.J. McClements, Biopolymer-based nanoparticles and microparticles: Fabrication, characterization, and application, Curr Opin Colloid Interface Sci. 19 (2014) 417–427. https://doi.org/10.1016/J.COCIS.2014.07.002.

[5] A. Araiza-Calahorra, A. Sarkar, Pickering emulsion stabilized by protein nanogel particles for delivery of curcumin: Effects of pH and ionic strength on curcumin retention, Food Structure. 21 (2019) 100113. https://doi.org/10.1016/J.FOOSTR.2019.100113.

[6] R.S. Hosseini, A. Rajaei, Potential Pickering emulsion stabilized with chitosan-stearic acid nanogels incorporating clove essential oil to produce fish-oil-enriched mayonnaise, Carbohydr Polym. 241 (2020) 116340. https://doi.org/10.1016/J.CARBPOL.2020.116340.

[7] T.K. Nguyen, H. Negishi, S. Abe, T. Ueno, Construction of supramolecular nanotubes from protein crystals, Chem Sci. 10 (2019) 1046–1051. https://doi.org/10.1039/C8SC04167A.

[8] N. Devi, M. Sarmah, B. Khatun, T.K. Maji, Encapsulation of active ingredients in polysaccharide–protein complex coacervates, Adv Colloid Interface Sci. 239 (2017) 136–145. https://doi.org/10.1016/J.CIS.2016.05.009.

[9] A. Madene, M. Jacquot, J. Scher, S. Desobry, Flavour encapsulation and controlled release – a review, Int J Food Sci Technol. 41 (2006) 1–21. https://doi.org/10.1111/J.1365-2621.2005.00980.X.

[10] S.H. Hu, C.H. Tsai, C.F. Liao, D.M. Liu, S.Y. Chen, Controlled rupture of magnetic polyelectrolyte microcapsules for drug delivery, Langmuir. 24 (2008) 11811–11818. https://doi.org/10.1021/LA801138E/SUPPL_FILE/LA801138E_SI_001.PDF.

[11] S.N. Pawar, K.J. Edgar, Alginate derivatization: a review of chemistry, properties and applications, Biomaterials. 33 (2012) 3279–3305. https://doi.org/10.1016/J.BIOMATERIALS.2012.01.007.

[12] M. Mancini, M. Moresi, R. Rancini, Uniaxial compression and stress relaxation tests on alginate gels, J Texture Stud. 30 (1999) 639–657. https://doi.org/10.1111/J.1745-4603.1999.TB00235.X.

[13] J. Burgain, C. Gaiani, M. Linder, J. Scher, Encapsulation of probiotic living cells: From laboratory scale to industrial applications, J Food Eng. 104 (2011) 467–483. https://doi.org/10.1016/J.JFOODENG.2010.12.031.

[14] S.C. Chew, K.L. Nyam, Microencapsulation of kenaf seed oil by co-extrusion technology, J Food Eng. 175 (2016) 43–50. https://doi.org/10.1016/J.JFOODENG.2015.12.002.

[15] D. Schell, C. Beermann, Fluidized bed microencapsulation of Lactobacillus reuteri with sweet whey and shellac for improved acid resistance and in-vitro gastro-intestinal survival, Food Research International. 62 (2014) 308–314. https://doi.org/10.1016/J.FOODRES.2014.03.016.

[16] A.R. Patel, D. Schatteman, W.H. De Vos, K. Dewettinck, Shellac as a natural material to structure a liquid oil-based thermo reversible soft matter system, RSC Adv. 3 (2013) 5324–5327. https://doi.org/10.1039/C3RA40934A.

[17] A. Samir, F.H. Ashour, A.A.A. Hakim, M. Bassyouni, Recent advances in biodegradable polymers for sustainable applications, Npj Materials Degradation 2022 6:1. 6 (2022) 1–28. https://doi.org/10.1038/s41529-022-00277-7.

[18] G. Ben Messaoud, L. Sánchez-González, L. Probst, C. Jeandel, E. Arab-Tehrany, S. Desobry, Physico-chemical properties of alginate/shellac aqueous-core capsules: Influence of membrane architecture on riboflavin release, Carbohydr Polym. 144 (2016) 428–437. https://doi.org/10.1016/J.CARBPOL.2016.02.081.

[19] M.P. Silva, F.L. Tulini, M.M. Ribas, M. Penning, C.S. Fávaro-Trindade, D. Poncelet, Microcapsules loaded with the probiotic Lactobacillus paracasei BGP-1 produced by co-extrusion technology using alginate/shellac as wall material: Characterization and evaluation of drying processes, Food Res Int. 89 (2016) 582–590. https://doi.org/10.1016/J.FOODRES.2016.09.008.

[20] E. Morales, M. Rubilar, C. Burgos-Díaz, F. Acevedo, M. Penning, C. Shene, Alginate/Shellac beads developed by external gelation as a highly efficient model system for oil encapsulation with intestinal delivery, Food Hydrocoll. 70 (2017) 321–328. https://doi.org/10.1016/j.foodhyd.2017.04.012.

[21] M. Minekus, M. Alminger, P. Alvito, S. Ballance, T. Bohn, C. Bourlieu, F. Carrière, R. Boutrou, M. Corredig, D. Dupont, C. Dufour, L. Egger, M. Golding, S. Karakaya, B. Kirkhus, S. Le Feunteun, U. Lesmes, A. MacIerzanka, A. MacKie, S. Marze, D.J. McClements, O. Ménard, I. Recio, C.N. Santos, R.P. Singh, G.E. Vegarud, M.S.J. Wickham, W. Weitschies, A. Brodkorb, A standardised static in vitro digestion method suitable for food – an international consensus, Food Funct. 5 (2014) 1113–1124. https://doi.org/10.1039/C3FO60702J.

[22] Q. Xu, H. Hong, J. Wu, X. Yan, Bioavailability of bioactive peptides derived from food proteins across the intestinal epithelial membrane: A review, Trends Food Sci Technol. 86 (2019) 399–411. https://doi.org/10.1016/J.TIFS.2019.02.050.

[23] F.B. Pimentel, M. Cermeño, T. Kleekayai, P.A. Harnedy, R.J. FitzGerald, R.C. Alves, M.B.P.P. Oliveira, Effect of in vitro simulated gastrointestinal digestion on the antioxidant activity of the red seaweed *Porphyra dioica*, Food Research International. 136 (2020) 109309. https://doi.org/10.1016/J.FOODRES.2020.109309.

[24] W. Li, H.-N. Su, Y. Pu, J. Chen, L.-N. Liu, Q. Liu, S. Qin, Phycobiliproteins: Molecular structure, production, applications, and prospects, Biotechnol Adv. 37 (2019) 340–353. https://doi.org/https://doi.org/10.1016/j.biotechadv.2019.01.008.

[25] R. Thangam, S. Sundarraj, R. Vivek, V. Suresh, S. Sivasubramanian, M. Paulpandi, S.V. Karthick, A.S. Ragavi, S. Kannan, Theranostic potentials of multifunctional chitosan-silver-phycoerythrin

nanocomposites against triple negative breast cancer cells, RSC Adv. 5 (2015). https://doi.org/10.1039/c4ra14043e.

[26] N. Senthilkumar, R. Thangam, P. Murugan, V. Suresh, C. Kurinjimalar, G. Kavitha, S. Sivasubramanian, R. Rengasamy, Hepato-protective effects of R-phycoerythrin-rich protein extract of *Portieria hornemannii* (Lyngbye) Silva against DEN-induced hepatocellular carcinoma, J Food Biochem. 42 (2018) 1–11. https://doi.org/10.1111/jfbc.12695.

[27] S. Ulagesan, T.J. Nam, Y.H. Choi, Extraction and Purification of R-Phycoerythrin Alpha Subunit from the Marine Red Algae Pyropia Yezoensis and Its Biological Activities, Molecules 2021, Vol. 26, Page 6479. 26 (2021) 6479. https://doi.org/10.3390/MOLECULES26216479.

[28] P. Castro-Varela, P.S.M. Celis-Pla, F.L. Figueroa, M. Rubilar, Highly Efficient Water-Based Extraction of Biliprotein R-Phycoerythrin From Marine the Red-Macroalga *Sarcopeltis skottsbergii* by Ultrasound and High-Pressure Homogenization Methods, Front Mar Sci. 0 (2022) 988. https://doi.org/10.3389/FMARS.2022.877177.

[29] A. Bennett, L. Bogobad, Complementary chromatic adaptation in a filamentous blue-green alga, Journal of Cell Biology. 58 (1973) 419–435. https://doi.org/10.1083/jcb.58.2.419.

[30] X. Ge, Z. Wan, N. Song, A. Fan, R. Wu, Efficient methods for the extraction and microencapsulation of red pigments from a hybrid rose, J Food Eng. 94 (2009) 122–128. https://doi.org/10.1016/J.JFOODENG.2009.02.021.

[31] E.S. Chan, Preparation of Ca-alginate beads containing high oil content: Influence of process variables on encapsulation efficiency and bead properties, Carbohydr Polym. 84 (2011) 1267–1275. https://doi.org/10.1016/J.CARBPOL.2011.01.015.

[32] C. Alarcon, C. Shene, Arduino Soft Sensor for Monitoring *Schizochytrium* sp. Fermentation, a Proof of Concept for the Industrial Application of Genome-Scale Metabolic Models in the Context of Pharma 4.0, Processes. 10 (2022) 2226. https://doi.org/10.3390/pr10112226.

[33] E. Rivas-Montoya, J. Miguel Ochando-Pulido, J. Manuel López-Romero, A. Martinez-Ferez, Application of a novel gastrointestinal tract simulator system based on a membrane bioreactor (SimuGIT) to study the stomach tolerance and effective delivery enhancement of nanoencapsulated macelignan, Chem Eng Sci. 140 (2016) 104–113. https://doi.org/10.1016/J.CES.2015.10.006.

[34] A. Brodkorb, L. Egger, M. Alminger, P. Alvito, R. Assunção, S. Ballance, T. Bohn, C. Bourlieu-Lacanal, R. Boutrou, F. Carrière, A. Clemente, M. Corredig, D. Dupont, C. Dufour, C. Edwards, M. Golding, S. Karakaya, B. Kirkhus, S. Le Feunteun, U. Lesmes, A. Macierzanka, A.R. Mackie, C. Martins, S. Marze, D.J. McClements, O. Ménard, M. Minekus, R. Portmann, C.N. Santos, I. Souchon, R.P. Singh, G.E. Vegarud, M.S.J. Wickham, W. Weitschies, I. Recio, INFOGEST static in vitro simulation of gastrointestinal food digestion, Nat Protoc. 14 (2019) 991–1014. https://doi.org/10.1038/s41596-018-0119-1.

[35] P. Abad, N. Arroyo-Manzanares, E. Rivas-Montoya, J.M. Ochando-Pulido, E. Guillamon, A.M. García-Campaña, A. Martinez-Ferez, Effects of different vehiculization strategies for the allium derivative propyl propane thiosulfonate during dynamic simulation of the pig gastrointestinal tract, Can J Anim Sci. 99 (2019) 244–253. https://doi.org/10.1139/CJAS-2018-0063/SUPPL_FILE/CJAS-2018-0063SUPPLA.DOCX.

[36] E. González, A.M. Gómez-Caravaca, B. Giménez, R. Cebrián, M. Maqueda, A. Martínez-Férez, A. Segura-Carretero, P. Robert, Evolution of the phenolic compounds profile of olive leaf extract encapsulated by spray-drying during in vitro gastrointestinal digestion, Food Chem. 279 (2019) 40–48. https://doi.org/10.1016/J.FOODCHEM.2018.11.127.

[37] M.T. Ariza, P. Reboredo-Rodríguez, L. Cervantes, C. Soria, E. Martínez-Ferri, C. González-Barreiro, B. Cancho-Grande, M. Battino, J. Simal-Gándara, Bioaccessibility and potential bioavailability of phenolic compounds from achenes as a new target for strawberry breeding programs, Food Chem. 248 (2018) 155–165. https://doi.org/10.1016/J.FOODCHEM.2017.11.105.

[38] W. Wang, R. Vignani, M. Scali, M. Cresti, A universal and rapid protocol for protein extraction from recalcitrant plant tissues for proteomic analysis, Electrophoresis. 27 (2006) 2782–2786. https://doi.org/10.1002/ELPS.200500722.

[39] U.K. Laemmli, Cleavage of Structural Proteins during the Assembly of the Head of Bacteriophage T4, Nature 1970 227:5259. 227 (1970) 680–685. https://doi.org/10.1038/227680a0.

[40] R.T. Abdala Díaz, V. Casas Arrojo, M.A. Arrojo Agudo, C. Cárdenas, S. Dobretsov, F.L. Figueroa, Immunomodulatory and Antioxidant Activities of Sulfated Polysaccharides from *Laminaria ochroleuca*, *Porphyra umbilicalis*, and *Gelidium corneum*, Marine Biotechnology. 21 (2019). https://doi.org/10.1007/s10126-019-09905-x.

[41] G. Indrayanto, G.S. Putra, F. Suhud, Validation of in-vitro bioassay methods: Application in herbal drug research, Profiles Drug Subst Excip Relat Methodol. 46 (2021) 273–307. https://doi.org/10.1016/BS.PODRM.2020.07.005.

[42] C. Juin, J.R. Chérouvrier, V. Thiéry, A.L. Gagez, J.B. Bérard, N. Joguet, R. Kaas, J.P. Cadoret, L. Picot, Microwave-assisted extraction of phycobiliproteins from *Porphyridium purpureum*, Appl Biochem Biotechnol. 175 (2015). https://doi.org/10.1007/s12010-014-1250-2.

[43] M. Jacotet-Navarro, N. Rombaut, S. Deslis, A.S. Fabiano-Tixier, F.X. Pierre, A. Bily, F. Chemat, Towards a “dry” bio-refinery without solvents or added water using microwaves and ultrasound for total valorization of fruit and vegetable by-products, Green Chemistry. 18 (2016). https://doi.org/10.1039/c5gc02542g.

[44] T. Pereira, S. Barroso, S. Mendes, R.A. Amaral, J.R. Dias, T. Baptista, J.A. Saraiva, N.M. Alves, M.M. Gil, Optimization of phycobiliprotein pigments extraction from red algae *Gracilaria gracilis* for substitution of synthetic food colorants, Food Chem. 321 (2020) 126688. https://doi.org/10.1016/j.foodchem.2020.126688.

[45] W. Pan-utai, S. Iamtham, Journal of King Saud University – Science Physical extraction and extrusion entrapment of C-phycocyanin from *Arthrospira platensis*, J King Saud Univ Sci. (2018). https://doi.org/10.1016/j.jksus.2018.05.026.

[46] M. Yan, B. Liu, X. Jiao, S. Qin, Preparation of phycocyanin microcapsules and its properties, Food and Bioproducts Processing. 92 (2014) 89–97. https://doi.org/10.1016/J.FBP.2013.07.008.

[47] S. Henning, S. Leick, M. Kott, H. Rehage, D. Suter, Sealing liquid-filled pectinate capsules with a shellac coating, J Microencapsul. 29 (2012) 147–155. https://doi.org/10.3109/02652048.2011.635220.

[48] E.S. Chan, B.B. Lee, P. Ravindra, D. Poncelet, Prediction models for shape and size of ca-alginate macrobeads produced through extrusion–dripping method, J Colloid Interface Sci. 338 (2009) 63–72. https://doi.org/10.1016/J.JCIS.2009.05.027.

[49] J. Stack, P.R. Tobin, A. Gietl, P.A. Harnedy, D.B. Stengel, R.J. FitzGerald, Seasonal variation in nitrogenous components and bioactivity of protein hydrolysates from *Porphyra dioica*, Journal of Applied Phycology 2017 29:5. 29 (2017) 2439–2450. https://doi.org/10.1007/S10811-017-1063-0.

[50] Q. Wu, X.P. Fu, L.C. Sun, Q. Zhang, G.M. Liu, M.J. Cao, Q.F. Cai, Effects of physicochemical factors and in vitro gastrointestinal digestion on antioxidant activity of R-phycoerythrin from red algae Bangia fusco-purpurea, Int J Food Sci Technol. 50 (2015) 1445–1451. https://doi.org/10.1111/IJFS.12775.

[51] Y. Yabuta, H. Fujimura, C.S. Kwak, T. Enomoto, F. Watanabe, Antioxidant Activity of the Phycoerythrobilin Compound Formed from a Dried Korean Purple Laver (*Porphyra* sp.) during in Vitro Digestion, Food Sci Technol Res. 16 (2010) 347–352. https://doi.org/10.3136/FSTR.16.347.

[52] J. Teixé-Roig, G. Oms-Oliu, S. Ballesté-Muñoz, I. Odriozola-Serrano, O. Martín-Belloso, Encapsulation and controlled release of phycocyanin during the in vitro digestion using polysaccharide-added double emulsions (W1/O/W2), Food Structure. 31 (2022) 100249. https://doi.org/10.1016/J.FOOSTR.2021.100249.

[53] M. Campos Assumpção de Amarante, A.R. Cavalcante Braga, L. Sala, S. Juliano Kalil, Colour stability and antioxidant activity of C-phycocyanin-added ice creams after in vitro digestion, Food Research International. 137 (2020) 109602. https://doi.org/10.1016/J.FOODRES.2020.109602.

[54] K.Y. Lee, D.J. Mooney, Alginate: properties and biomedical applications, Prog Polym Sci. 37 (2012) 106. https://doi.org/10.1016/J.PROGPOLYMSCI.2011.06.003.

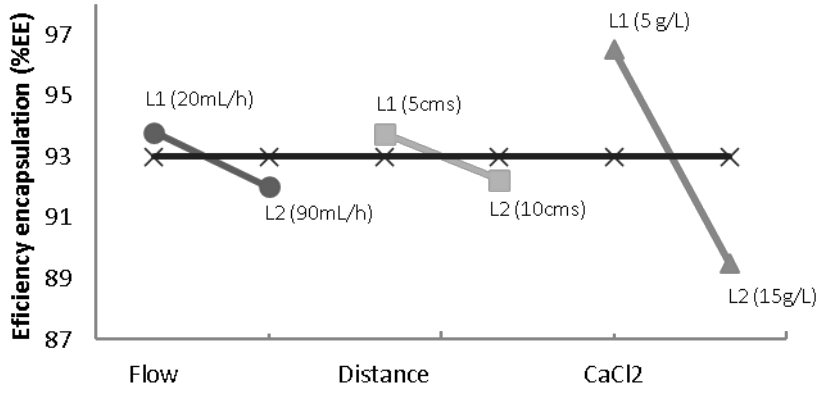

Working Levels	(Flow)	(Distance)	($CaCl_2$)
L1	93.25	93.75	96.5
L2	92.75	92.25	89.5
Difference ΔL(1,2)	0.5	1.50	7.0

Figure 1. Effect of the working levels of each variable on the encapsulation efficiency.

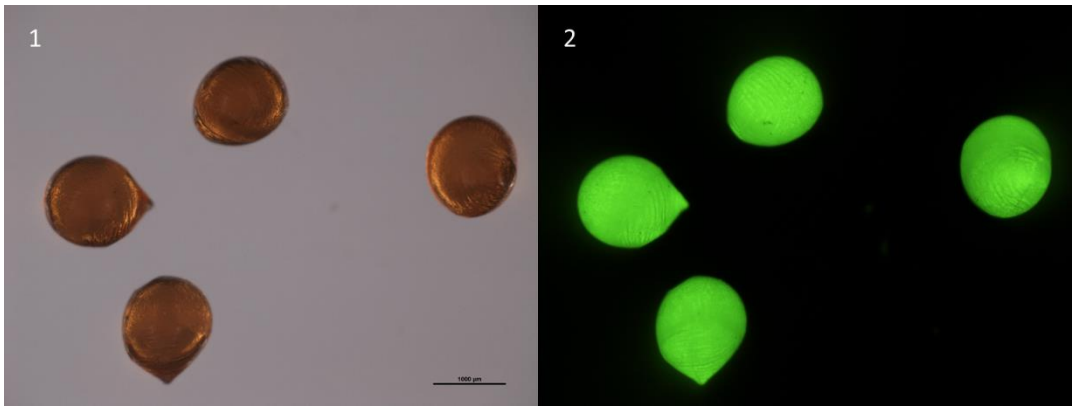

Figure 2. Confocal microscopic for 1) design point N°1 (97.5%EE) and 2) presence of R-phycoerythrin by fluorescence.

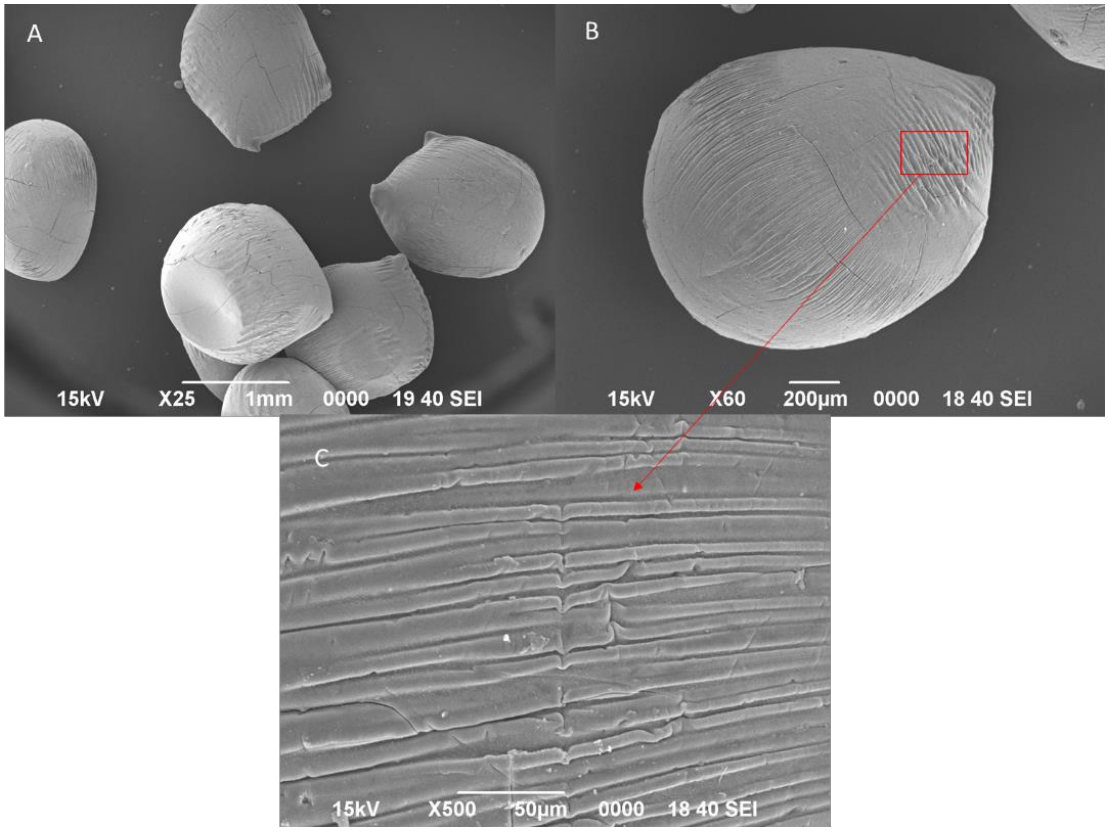

Figure 3. Morphology of the beads by scanning microscopy (SEM) for a) design point N°1, b) design point N°4, and c) magnification of 500X for the surface of the beads of design point N°4.

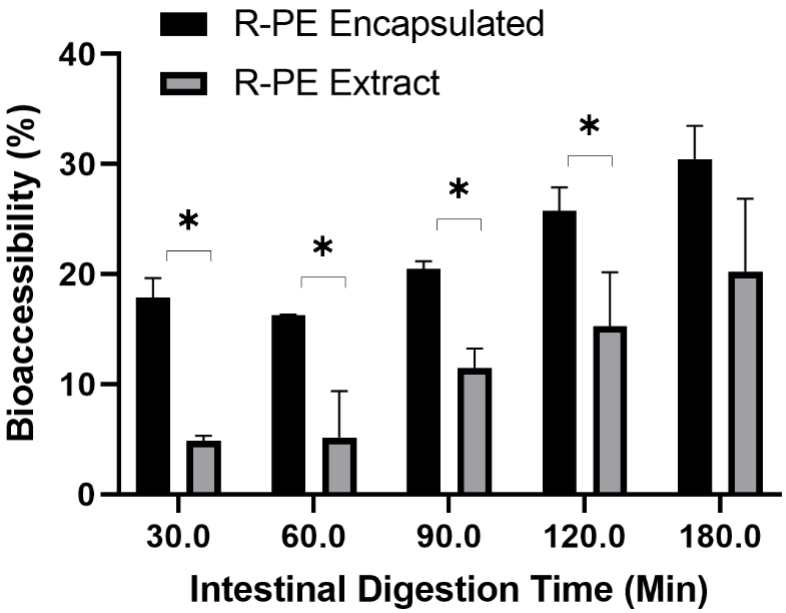

Figure 4.Bioaccessibility (%) of R-PE extract and encapsulated R-PE during in vitro gastrointestinal digestion. Bars with an asterisk indicate a significant difference ($p<0.05$) between encapsulated R-PE and R-PE extract.

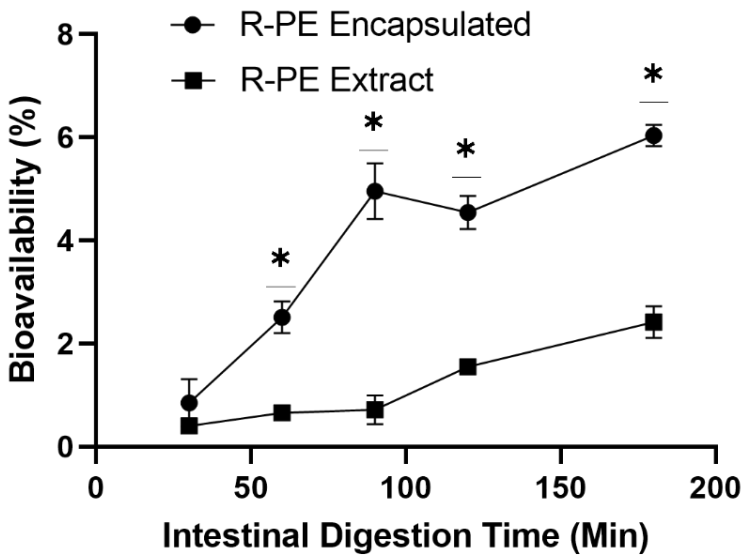

Figure 5. Bioavailability (%) of R-PE extract and encapsulated R-PE during *in vitro* gastrointestinal digestion. A line with an asterisk indicates a significant difference ($p<0.05$) between encapsulated R-PE and R-PE extract.

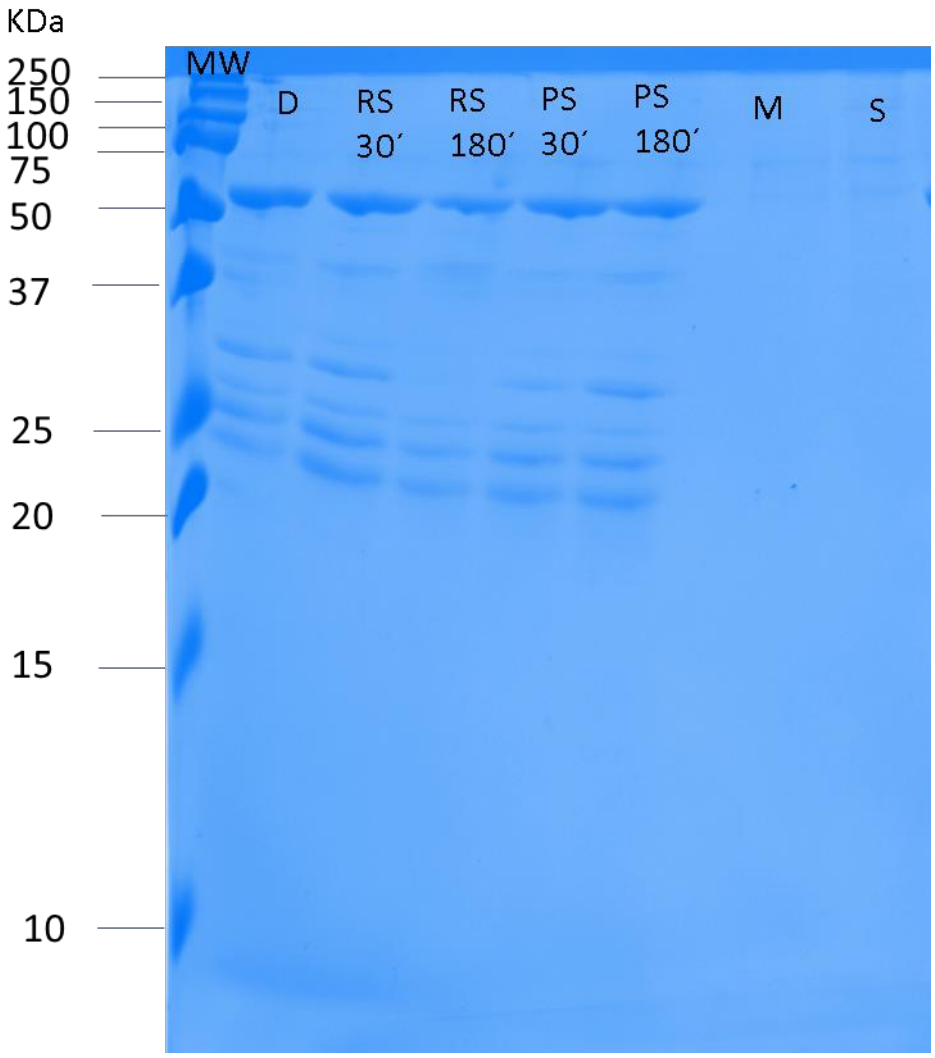

Figure 6. Sodium dodecyl sulfate polyacrylamide gel electrophoresis (SDS-PAGE) profile of encapsulated R-PE from a different stage of *in vitro* simulated digestion (simuGIT). 50µg of protein were loaded into the corresponding lane. MW: Molecular weight marker; D: Duoden; RS30´: Retentate streams at 30min; RS180´: Retentate streams at 180min; PS30´: Permeate streams at 30min; PS180´: Permeate streams at 180min; M: Mouth; S: Stomach.

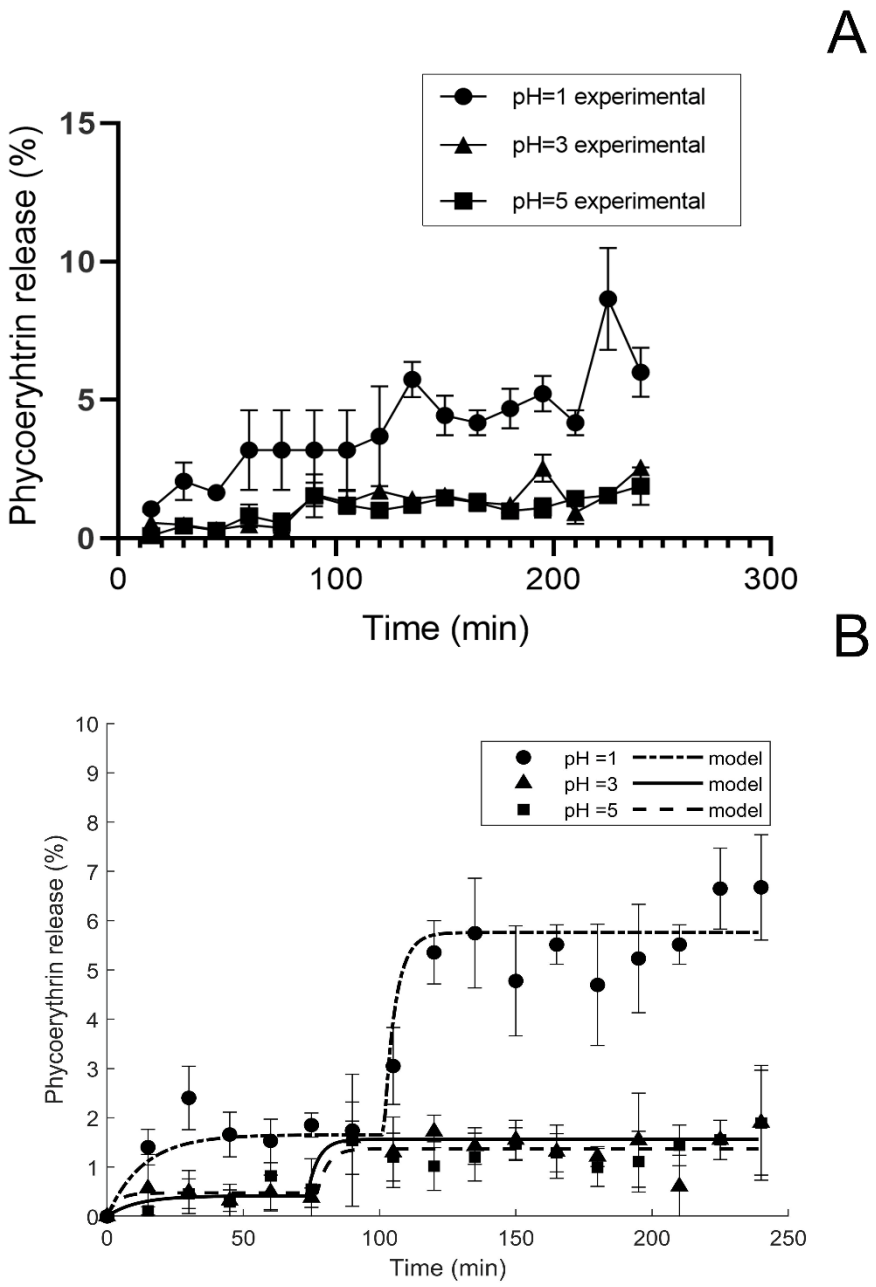

Figure 7. Phycoerythrin release as a percentage of total with respect to time, A) Experimental R-PE release from alginate/shellac capsules during 250min at different pH values. Points with asterisks indicate significant differences ($p<0.05$). B) modeled using a second-order differential equation representing a two-step first-order release response.

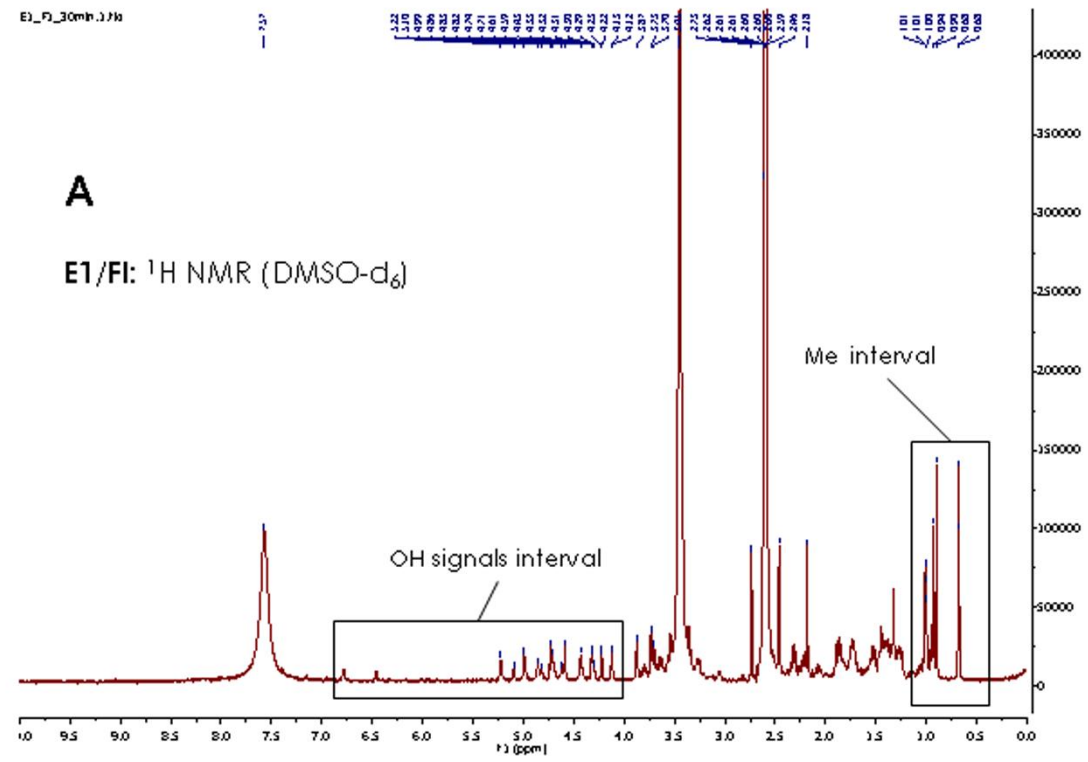

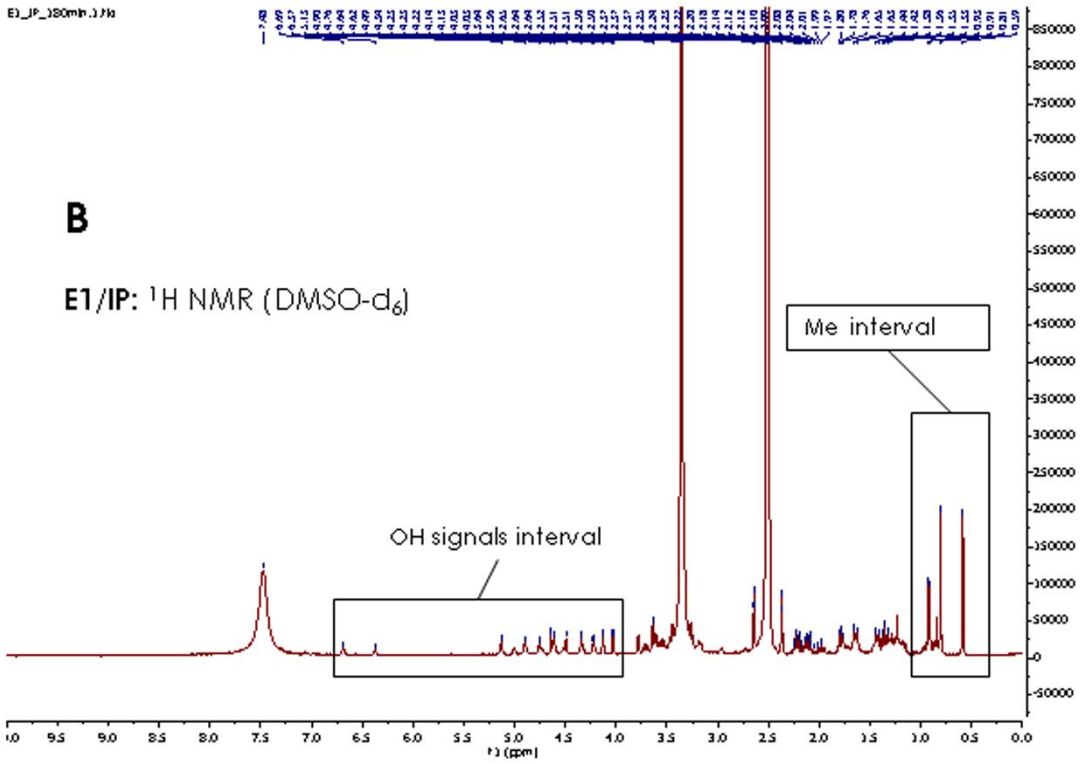

1048 Figure 8. ^{1}H NMR (DMSO-d$_6$) spectra of E1/FI (A) and E1/IP (B) samples. E1/FI: Evaluation
1049 of intestinal fraction concentred. E1/IP: Evaluation of intestinal fraction permeated.

Table 1. Encapsulation efficiency of R-PE, sphericity factor, and particle size using the orthogonal matrix L_4 (2^3).

Design point	Orthogonal Matrix L4 (2^3)			Characterization of beads		Encapsulation efficiency
	Flow (mL h^{-1})	Distance (cm)	$CaCl_2$ (gr L^{-1})	Sphericity factor (SF)	Size (mm)	%EE
1	20 (L_1)	5 (L_1)	5 (L_1)	0.06 ± 0.02	1.2 ± 0.2	97.5 ± 0.7
2	20 (L_1)	10 (L_2)	15 (L_2)	0.10 ± 0.03	1.6 ± 0.1	89 ± 1.41
3	90 (L_2)	5 (L_1)	15 (L_2)	0.09 ± 0.05	1.1 ± 0.2	90 ± 1.41
4	90 (L_2)	10 (L_2)	5 (L_1)	0.07 ± 0.01	1.1 ± 0.1	95.5 ± 0.71

Table 2. Cytotoxicity index (IC_{50}) and selective index (SI) for encapsulated and non-encapsulated R-PE on the different cell lines: 1064 sK (human gingival fibroblast cell line), HCT-116 (human colon cancer), G-361 (human melanoma), U-937 (human leukemia).

Samples	Health and Antiproliferative active cell lines	Cytotoxicity Index IC_{50} (μg mL^{-1}).	Selectivity Index (SI)
Encapsulated	1064sK	3516 ±15.3	-
	HCT-116	1076 ± 8.46	3.27
	U-937	1251 ± 4.83	0.86
	G-361	4132 ± 10.86	0.26
Non-Encapsulated (R-PE extract)	1064sK	4438 ± 10.3	-
	HCT-116	144.5 ± 3.96	30.71
	U-937	2702 ±12.6	1.59
	G-361	2788 ±11.5	1.64

Table 3: Parameters for the second order model for Phycoerythrin release.

	a_1	a_2	c_1	c_2	t_d	NRMSE
pH=1	0.125	0.995	0.075	0.243	101.573	15.944
pH=3	0.038	0.297	0.092	0.258	73.452	28.948
pH=5	0.130	0.239	0.273	0.266	77.107	24.870

Table 4: Response of release of pigment.

	max release stage 1	max value stage 2	Stabilization time stage 1 (min)	Stabilization time stage 2 (min)	Time delay
pH=1	1.657	5.758	66.490	20.617	101.573
pH=3	0.416	1.565	54.571	19.357	73.452
pH=5	0.476	1.371	18.315	18.765	77.107

CONFLICT OF INTEREST

The authors declare that there are no conflicts of interest.

BIOETHICAL APPROVALS

Experiments were conducted under notifications A/ES/12/I-22 and A/ES/12/24 to Ministry of Ecological Transition and Demographic Challenge and approval 100-2018-T of the UMA Bioethics commission.

CRediT author statement

Conceptualization, P.C-V., M.R., F.L.F. and R.A-D.; methodology C.A. and P.C-V.; mathematical model methodology and Taguchi optimization, C.A; SIMUGIT methodology, A.M-F.; SIMUGIT supervision and writing A.M-F.; NMR methodology, D.F-R and J.M.L.; NMR experiment supervision and writing, J.M.L; data curation, C.A and P.C-V; validation, P.C-V; writing original draft preparation, P.C-V.; writing-review and editing, P.C-V., M.R., F.L.F. J.M.L., A.M-F., and R.A-D.; visualization, P.C-V; supervision, M.R., F.L.F. and R.A-D. All authors have read and agreed to the published version of the manuscript.